Image Analysis for Object Detection in Millimetre-wave Images

Christopher D. Haworth[a], Beatriz Grafulla González[a], Mathilde Tomsin[a], Roger Appleby[b], Peter Coward[b], Andrew Harvey[a], Katia Lebart[a], Yvan Petillot[a], Emanuele Trucco[a]

[a]Heriot-Watt University, Edinburgh, UK
[b]QinetiQ, Malvern, UK

ABSTRACT

Video-frame-rate millimetre-wave imaging has recently been demonstrated with a quality similar to that of a low-quality uncooled thermal imager. In this paper we will discuss initial investigations into the transfer of image processing algorithms from more mature imaging modalities to millimetre-wave imagery.

The current aim is to develop body segmentation algorithms for use in object detection and analysis. However, this requires a variety of image processing algorithms from different domains, including image de-noising, segmentation and motion tracking. This paper focuses on results from the segmentation of a body from the millimetre-wave images and a qualitative comparison of different approaches is presented. Their performance is analysed and any characteristics which enhance or limit their application are discussed.

While it is possible to apply image processing algorithms developed for the visible-band directly to millimetre-wave images, the physics of the image formation process is very different. This paper discusses the potential for exploiting an understanding of the physics of image formation in the image segmentation process to enhance classification of scene components and, thereby, improve segmentation performance. This paper presents some results from a millimetre-wave image formation simulator, including synthetic images with multiple objects in the scene.

Keywords: millimetre-wave, image formation, image processing

1. INTRODUCTION

Millimetre-wave imaging has seen a significant number of advances over the last couple of years as a surveillance technology. In particular, a video-frame-rate millimetre-wave imager has recently been demonstrated with a quality similar to that of a low-quality uncooled thermal imager.[1] This presents the possibility of applying millimetre-wave imaging to a wider range of applications, including the detection of concealed objects within a scene. A suitable application could be a generic entry-security system, in which it is common practise to employ a gateway metal detector. In this case the given scene would be a single subject standing or moving in front of the imager and the system would be designed to detect any foreign objects being carried by the subject.

This paper is divided into three sections. The first section introduces the millimetre-wave (MMW) imager employed in this work and outlines the proposed system and its application to real-world situations. The second section examines the underlying behaviour of the MMW images and provides approaches for statistical analysis which can be deployed for de-noising and image segmentation for object detection. Section 4 discusses an approach using the statistically-learnt Active Shape Models[2] to segment the image into background and subject.

The final section of the paper discusses the physics behind millimetre-wave image formation that is incorporated into scene simulation. Conclusions are then presented about the future direction and applicability of this work.

Further author information: (Send correspondence to C D Haworth or B Grafulla González)
C D Haworth: E-mail: C.D.Haworth@hw.ac.uk, Telephone: +44 (0) 131 451 3299
B Grafulla González: E-mail: bg5@hw.ac.uk, Telephone: +44 (0) 131 451 3299

2. MMW TECHNOLOGY

2.1. QINETIQ MMW IMAGER

There are currently a number of fundamentally different technologies employed in state-of-the-art MMW imaging. The MMW imager employed in this work is a 1D scanned focal-plane array operating at 35GHz and is capable of producing real-time head-to-toe video output. However, due to the 1D construction of the imager software interpolation onto a 2D grid is required to produce the video output. The output resolution is roughly equivalent to Common Intermediate Format (320×240).

In outdoor applications it is not necessary to artificially irradiate subjects. For indoor applications, however, it is necessary to provide artificial illumination. An indoor illumination chamber suitable for use with the MMW imager has also been demonstrated,[3] which provides a reasonable approximation of the low-coherence directional illumination present outdoors increasing the contrast to hundreds of kelvins. Furthermore, it does not expose the subject to harmful radiation.

2.2. MMW IMAGER APPLICATIONS

It has previously been proposed that this technology be used in aviation security applications,[4] public event security[1] and detection of illegal passengers in lorries[5] with positive results in all trials. In this paper we will discuss initial investigations into the transfer of image processing algorithms from more mature imaging modalities to millimetre-wave imagery. The current aim is to develop algorithms for the detection and analysis of objects in MMW images.

An initial target application of public-entry security scanning has been chosen, which could be applicable in a wide variety of situations including aviation security. In this target application it is assumed initially that a stream of subjects are entering the scanner individually and rotating slowly through 360 degrees. Their time in the sensor, body position and motion are assumed to be supervised to allow suitable scanning.

In this system four key stages are required: to analyse and pre-process the image (image pre-process), segment the image into constituent parts (image segmentation), identify possible objects (candidate regions) and, finally, analyse the possible candidates (region analysis). The work presented in the remainder of this paper focuses on the first two stages of this system on image de-noising and image segmentation. Work is ongoing on all parts of the system and further results will be published soon. Work is also taking place on a privacy filter to allow human scanning of the MMW while maintaining the privacy of the subjects.

3. IMAGE STATISTICS

3.1. DISTRIBUTION FITTING

The first step in the design of the image pre-processing stage is an analysis of the underlying image statistics. The method chosen is one of fitting probability density functions (PDF) to the histogram of the image intensities. To select the PDF type it would be desirable to have an understanding of the physical process. However, given the complexity of the MMW imager and the extensive amount of hardware calibration, software equalisation and interpolation undertaken to produce a MMW image, the selection is performed manually.

A wide range of distribution models were tried, including Gaussian, Rayleigh, Weibull, Cauchy and Laplace. It can be seen from Figure 1 that while the histogram may appear Gaussian, a single Gaussian model does not provide an accurate fit. Instead a mixture of Gaussians, shown in Equation 1, provides a considerably more accurate fit of the empty, illuminated chamber.

$$PDF_{mix} = \phi * PDF_{gauss}(\mu_1, \sigma_1) + (1 - \phi) * PDF_{gauss}(\mu_2, \sigma_2) \tag{1}$$

However, when an object enters the scene a mixture of Gaussians model fails to provide an accurate fit within a reasonable number of parameters. After experimentation it was determined that two different distributions were required for fitting background and foreground. Rayleigh for the foreground and either a Gaussian or Laplace for the background. The results for these two combinations are shown in Figure 1, with the background, foreground and combined PDF illustrated. The dual PDF models provide a good trade off between accuracy

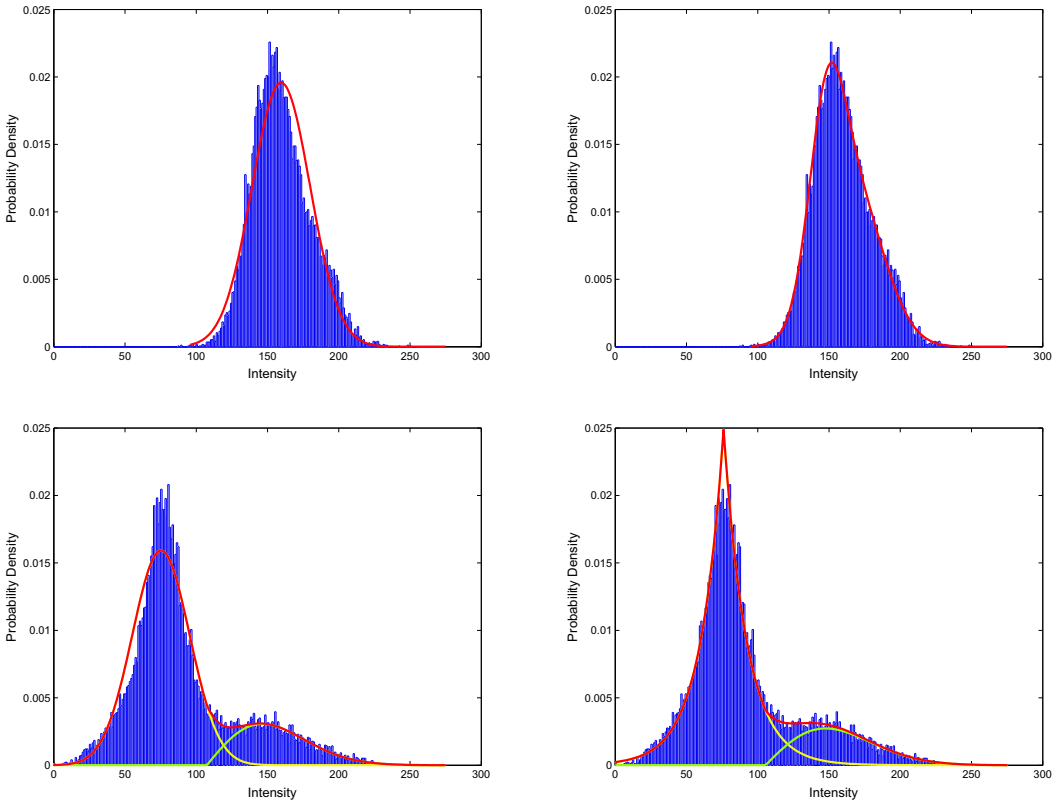

Figure 1. PDF fitting on an illuminated but empty chamber with a single Gaussian model (top left) and a dual Gaussian model (top right). PDF fitting on an illuminated chamber with subject using a combination Gaussian+Rayleigh (bottom left) and a combination Laplace+Rayleigh (bottom right).

and complexity. Note that all dual distribution models were constructed using the formation shown for the dual Gaussian model (Equation 1).

An interesting and useful extension to this piece of work would be to link the physics of MMW image formation with the PDF for the image data, perhaps through the use of a physical model of MMW image formation. However, this is beyond the scope of the paper and is not necessary for the subsequent image processing algorithms presented.

3.2. UNSUPERVISED SEGMENTATION

The analysis of underlying image statistics revealed a statistical difference between foreground and background intensities. Furthermore, the statistical model presented provides a natural basis for unsupervised image segmentation. A common class of simple unsupervised image segmentation algorithms attempt to group the data into k clusters through minimisation of the dispersion within each cluster using statistical measures. The simplest statistical measure sums the squared Euclidean distances from the mean of each cluster and this technique is called k-Means.[6]

Using a standard implementation of the k-Means algorithm the pixels are divided into k classes and the mean and standard deviation for each class are estimated. The mean and standard deviation of each class can be passed onto the distribution models, which in turn are used to identify the most likely class for each pixel. In this case the k-Means algorithm provides an estimate of the statistics of the k classes and a maximum-likelihood classification is performed on the image. The maximum-likelihood classification employs the PDF models developed in the previous section. This can be summarised as follows:

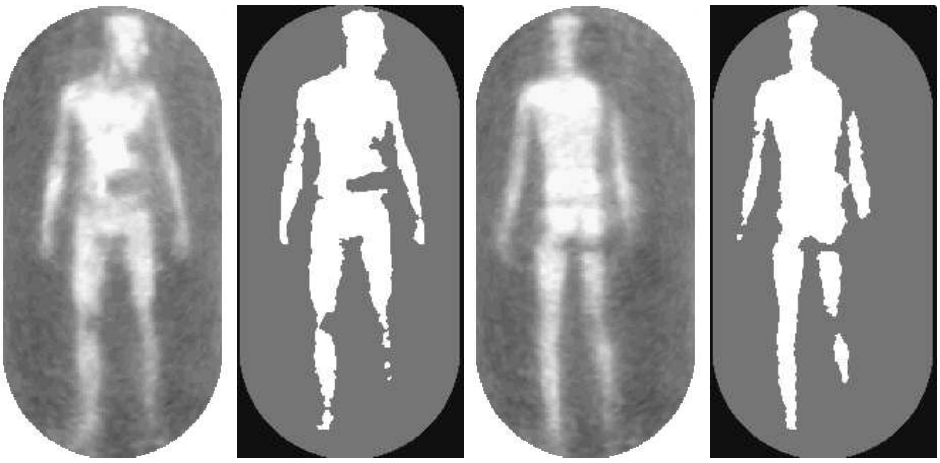

Figure 2. Example images from the *k*-Means segmentation algorithm showing both the original MMW images and the segmentation. The subject in the left figure has three objects on their person, visible in the MMW image as dark patches. Two objects are on the left hand-side of their torso and the third is located on the inside of the right knee.

1. Initial *k*-Means segmentation into classes
2. Statistics (μ, σ) estimated for each class
3. Maximum-likelihood classification using dual-PDF models

It can be seen from the results, shown in Figure 2, that a good quality segmentation of the subject has been achieved. The most common difficulty with this algorithm is associated with uneven illumination or shadows causing areas of the subject to blend into the background. It is unlikely that significant improvements could be made with alternative unsupervised classification algorithms without detailed use of model *priors*. This approach is addressed further in Section 4.

3.3. METALLIC OBJECT DETECTION

The analysis of the image statistics also suggested that given the current sensor equalisation / calibration process, intensity statistics differ when metal objects appear in the scene. It can be scene from the two histograms shown in the top row of Figure 3 that both the maximum intensity and overall distribution of values vary.

The difference (ratio) in maximum image intensity across the whole sequence was shown to provide consistent discrimination between scenes where a metallic object is / isn't present, for all data sequence currently available. The graphs on the bottom row of Figure 3 demonstrate this difference; a sharp step change indicates a metallic object has entered the scene. A Hidden Markov Model[7] can be trained to analyse the difference matrix across the sequence and recognise specific transitions from one state to another. This fine tuning allows the detailed detection of metallic objects that would not be possible with a rule-based thresholding technique because of the uncontrolled variations between sequences. The HMM implementation available in Matlab Statistics Toolbox was employed. To allow for a varying probability of an object being present in the scene it was decided to employ 10 states to represent the transition from the two discrete states of *present* and *absent*. Initial examination of the results suggests that the HMM is very successful in identifying metallic objects in the scene, with the system achieving 90% success in comparison to human ground truth.

Interestingly, applying this metallic object detection can dramatically improve the image segmentation. A number of assumptions must hold true for *k*-Means, which were presented in the previous section, to perform satisfactorily. In particular, the number of clusters must be known and the clusters must be circular, non-overlapping and non-hierarchical. It has already been demonstrated that the second assumption on cluster shape is met to an acceptable standard, with the results shown in Figure 2. However, as previously discussed,

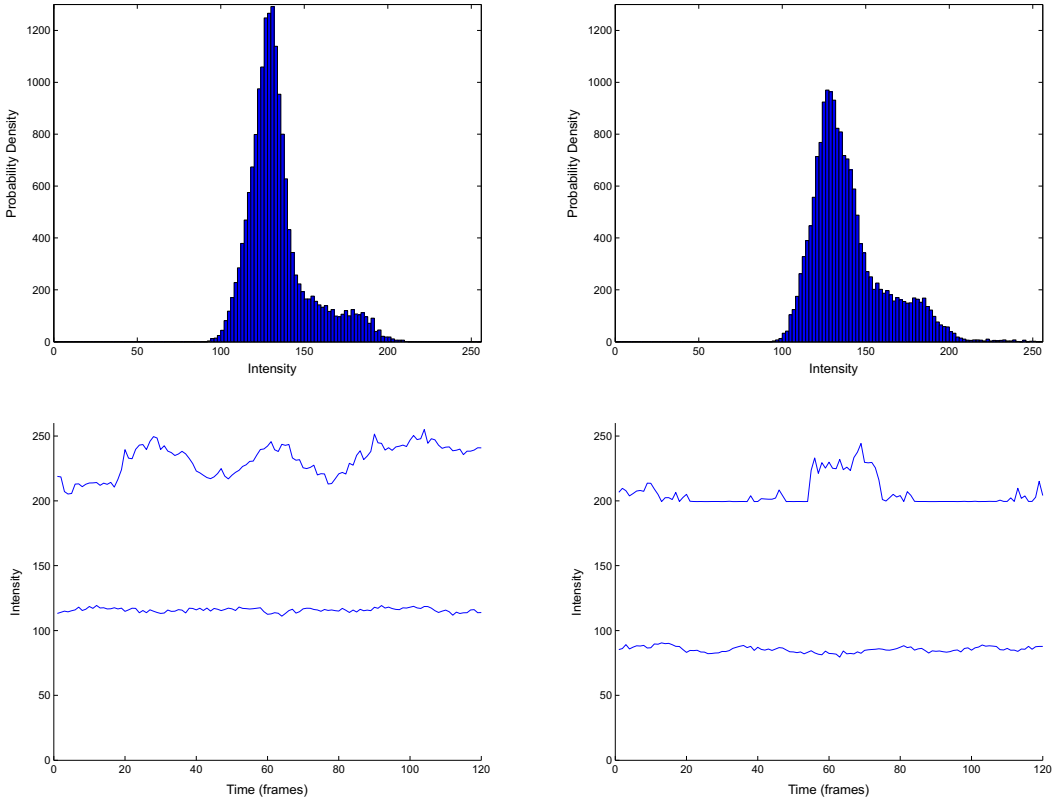

Figure 3. The top row shows histograms of image intensities taken from a single frame from a sequence with a subject in the scene (left) and a sequence with a subject carrying a gun (right). The bottom row contains the minimum and maximum image intensities across the entire sequence.

the scene statistics change when objects, in particular metallic objects, enter the scene. This can influence the number of clusters required.

The results of HMM detection of metallic objects can be used to initialise the k-Means segmentation with the correct number of clusters (k). Figure 4 shows a MMW image with two segmentations using two and three classes in the k-Means algorithm. It is clear from these results that it is important to know the correct number of classes in the scene. It can also be seen that a reasonable segmentation of the metallic object has taken place and that this segmentation could then be used to provide basic position, shape and motion of any objects in the scene to a tracking algorithm. Work on tracking is ongoing and further results will be reported. Recent relevant work is presented by Slamani *et al.*[8,9]

At present this work is highly dependent on the current calibration of the sensor and a robust method will need to be developed if this method is to be considered for future use. Furthermore, the range of object parameters (e.g. minimum object size) with which the system can cope will need to be investigated fully. However, the current method does demonstrate simple yet highly effective detection of metallic objects. An alternative method to be pursued in future work will be to investigate PDF fitting based on the variation in overall distributions seen in Figure 3, perhaps using Bayesian Information Criteria.[?]

4. MODEL-BASED SEGMENTATION

Deformable models are a common and well investigated techniques for image segmentation. Background information can be gained from previous literature on deformable models,[10] active contours[11] and active shape / appearance models.[2] The Active Shape Model (ASM) represents a parametric deformable model, constructed

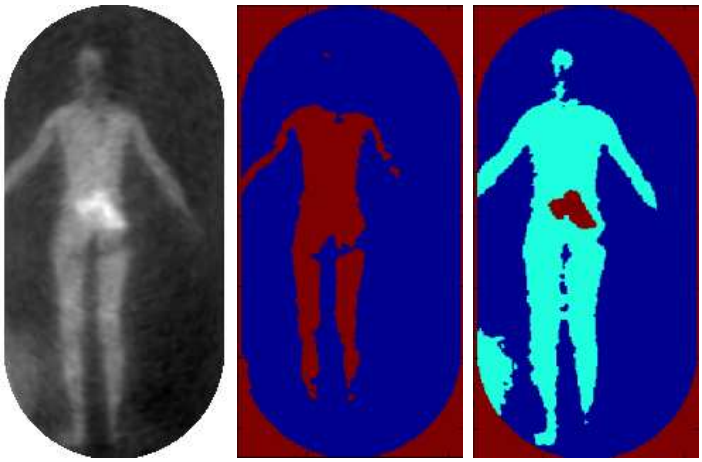

Figure 4. A MMW image (left) with two k-Means segmentations using too few clusters (centre) and correct number of clusters (right). The object in the bottom left of the scene is a metal sphere.

from contours, where a statistical model of the global shape variation from a training set is built. Careful design of the training set is necessary to allow generation of plausible shapes.

ASM segmentation requires two assumptions: that the ASM is initialised at a reasonable starting point and that the training set is sufficiently representative. Experience suggests that the two key items for initialisation in our application are accurate figure size (height) and accurate identification of the centre line of the body (spine). Using the earlier segmentation techniques, shown in Figure 2, and some basic assumptions on the subject starting position, it is possible to initialise the ASM accurately. However, for the second assumption on training sets, careful analysis of the parameters that are going to be tracked is necessary, which is discussed further in the next section.

4.1. ASM MODEL PARAMETERS

A key element in accurate use of the ASM is in the design of the training set, which in turn allows generation of plausible shapes. The target application presented in Section 2 where a subject enters the sensor, turns through 360 degrees while holding their arms fixed and then leaves, provides some strong prior information. This is important as monitoring human motion is extremely complex and use of all available knowledge necessary. A summary of the parameters required for this system are:

- Subject body shape and height (e.g. limb lengths, weight)
- Subject age and gender variation (e.g. child, male/female)
- Static pose variations (e.g. arm angle, leg placement)
- Moving 3D pose variations (e.g. subject rotation)

The first two parameters could be represented by prior information found in anthropomorphic data and are required to provide the ASM with a realistic set of contours for human body variation. The third parameter could be represented by a CAD-style human body model with a kinetic chain and is required to limit the body motion to a range of realistic movements; for example an elbow has a specific range of motion. While these first three parameters represent a significant amount of information on which the ASM would need trained, it is possible to isolate training data suitable for each parameter. However, the final parameter represents a significant and challenging problem because the Active Shape Models algorithm is based on a 2D image and it is assumed that every point on the model can be seen at all times. To overcome this problem Cootes *et al.*[12] demonstrated a technique with Active Appearance Models for tracking faces through 180 degrees using 6 separate models, each

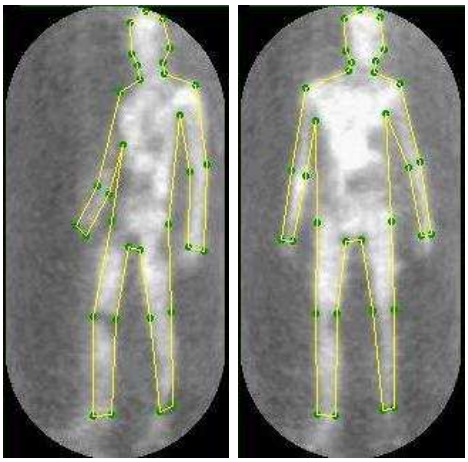

Figure 5. Two images from a sequence tracked using a trained ASM. It can be seen that the ASM has tracked the motion of the subject in a plausible manner. This example employs a small number of points but in practice a significantly larger number of points (approximately 100) has been found to be effective.

of which tracks a portion of the rotation. It is possible to adapt this design to work with ASM on a human figure rotation through 360 degrees. The one obvious difficulty in adapting this technique is the model selection criteria. In the original work an Active Appearance Model (AAM) was employed which reconstructs the entire image and the difference (residual) between the reconstructed image and input image was employed to select the most accurate model. In the case of an ASM only the contour is reconstructed and so no residual image will be available. However, the subject rotates in a predefined manner and any unusual movement would require the subject to be rescanned making the task of switching models considerably easier.

Importantly it is not the aim of the training set to replicate the division of parameters that a human would produce. Attempting to do so would defeat the purpose of employing the PCA reduction, where an efficient representation of the variation seen in the training set is searched for. However, it is important that no correspondence between independent parameters is implied through inadequate training. For this reason one must validate the PCA modes as independent.

4.2. ASM TRAINING AND TESTING

The first phase of testing of the ASM concentrated on the first three parameters with the aim of determining the efficiency of the ASM training and the likely training set required for full use. This represents a significant test for the ASM segmentation and will help determine its suitability for use on MMW images. The available training data consisted of seven sequences (5 males and 2 females) with each subject performing several rotations in the scene. A further seven sequences were available for testing this time with the subjects carrying an object. The objects included a set of keys, a mobile phone and a hand-gun.

The key advantage of an ASM is that given a suitable training set, an accurate segmentation can be achieved (Figure 5). Furthermore, the segmentation is based on the limbs allowing annotation of key body parts, which would be valuable in the implementation of a privacy filter. Another advantage is that complex model priors are not required; although this is somewhat offset by the large training set it is possible to aim for coverage through volume in the training set which is not possible with priors. However, the complexity of the training set required remains a significant problem, with any examples outside of the previous training resulting in very poor segmentation. Furthermore, in our application this failure tends to be catastrophic although this may actually aid in failure detection.

The key obstacles remaining are over-sensitivity to object size and complexity of utilising multiple models to cope with 3D rotation. The initialisation step is already required to align the 2D shape in translation and it is probable that it could also normalise the object size. However, the proposed system of multiple models for 3D tracking has not be fully tested and may prove complex to implement successfully.

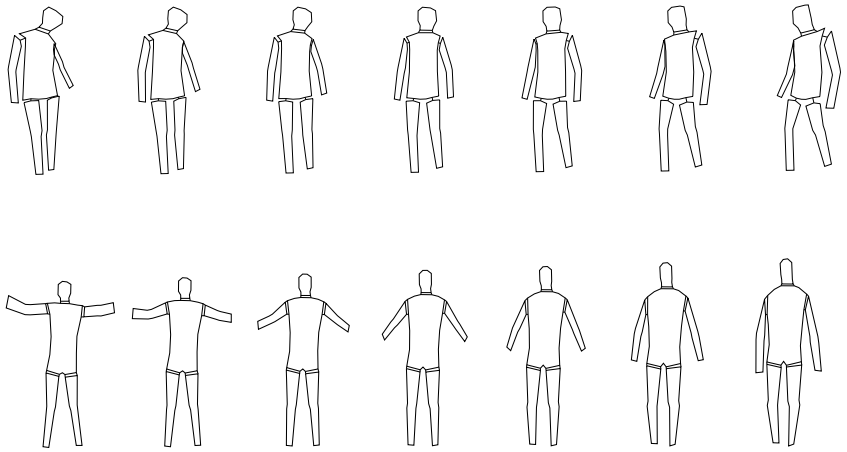

Figure 6. The first PCA mode from two different ASM models are shown. In the top PCA mode, from a correctly trained system, the PCA captures rotation as a significant variation. In the bottom PCA mode, from a under-trained system, the mode has mixed body height, body weight and arm angle.

The final difficulty with the training set is illustrated in Figure 6. This shows two PCA modes from two different ASM models, with the first from a correctly trained system and the second from an under-trained system. In the first example the mode represents a rotation of the entire body, with associated arm and leg motion. The mean body shape is shown with other body variations represented in other PCA modes in the ASM model. In the second example shown in Figure 6 the mode has confused multiple variations including body height, body weight and arm angle.

The conclusions that can be drawn from this work on ASM for MMW images is that the first three parameters, given in Section 4.1, provide a complex and challenging range of data over which the ASM has to be trained. The evidence so far suggests that a suitably large and well-chosen training set would enable Active Shape Models to cope with our problem. However, from recent related work[13] it is clear that there is a limit to the amount of data that can be learnt using this technique. For this reason, it is probable that further sub-division of the model space would be required. Some possible divisions would be gender-based, adult/child and weight. Given that each model would require 8 sub-models for rotation a very large number of models and, therefore, training sets may be required for accurate tracking. Early work on initialising the correct model has provided promising results but due to the significant time cost in capturing sequences and training the Active Shape Models alternative strategies are currently being investigated.

5. MILLIMETRE-WAVE IMAGES

There are three main motivations for being able to produce synthetic millimetre-wave images in this project. As seen before, most imaging techniques require a large amount of data, and image acquisition campaigns are costly to set up. Synthesising images further provides ground truth data (as the scene and its correspondence with the image is known) and full control off the scene. Lastly, an image simulation enables experimental control on the influence of different physical parameters of the sensor, therefore enabling to explore both the phenomenology of the image formation and possible changes in the sensor set up.

In this section, we discuss physics relevant to the image formation and outline how it has been used to develop a simulator of millimetre-wave images.

5.1. MILLIMETRE-WAVE IMAGE FORMATION

Two different phenomena come into play during the formation of millimetre-wave images; (1) the combination of power from various components present in the scene and (2) the modification of the recorded signal by the

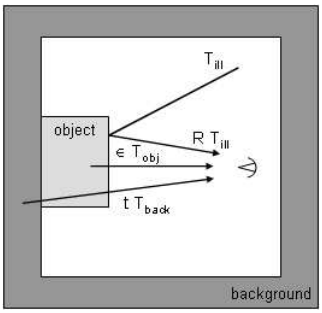

Figure 7. One of the different phenomena which come into play during the formation of millimetre-wave images: the combination of power from various components present in the scene. The second phenomenon deals with the modification of the recorded signal by the instrumental response, including the imager impulse response and noise effects.

instrumental response, including the imager impulse response and noise effects. This second component will not be considered here in depth. Hence, the objective of this section is to describe the different source intensities which influence the formation of millimetre-wave images.

The frequency at which the images are formed is $f = 35\ GHz$ or equivalently $\lambda \approx 9\ mm$. The focal ratio of the imager is $0.8\ m$ resulting in a diffraction-limited spot-size of $\sim 2.0\ cm$. We consider only a short-range indoor scene (the influence of the atmosphere is hence neglected) with incoherent illumination.

The temperature of the objects in the scene is above absolute zero which means that scene objects radiate power in the millimetre-wave range with an emissivity ϵ compared to the radiation of an ideal black body. Since the surfaces of the body and threats are flat on the scale of the wavelength, the reflections are considered specular. This implies that the scattering effects are small and propagation of light within the scene will obey ray optics approximations. The intensity of mm-wave radiation at each pixel is determined by contributions from both self-emission by scene components and by reflections from illumination sources both within and external to the scene. Illumination of the scene is by ambient background black body radiation with a temperature in the region of 290 K and by extended diffuse sources with elevated equivalent temperatures of, typically, 800 K. It is important to note that the reflectivity, R, the emissivity, ϵ, and the transmissivity t are related through Equation 2.

$$R + \epsilon + t = 1 \tag{2}$$

Moreover, these three coefficients depend on the physical characteristics of the materials defined via the dielectric constant ε, the permeability μ, the angle of incidence θ_i and the polarisation p (horizontal or vertical).

Since the source is incoherent, the three intensity coefficients in Equation 2 are added (Fig. 7), obtaining Equation 3 which describes the received temperature at the input of the sensor.

$$T_{rec}(\varepsilon, \mu, \theta, p) = R(\varepsilon, \mu, \theta, p) \cdot T_{ill} + \epsilon(\varepsilon, \mu, \theta, p) \cdot T_{obj} + t(\varepsilon, \mu, \theta, p) \cdot T_{back} \tag{3}$$

where ε is the dielectric constant, μ the permeability, θ the angle of incidence, p the polarisation, $R(\varepsilon, \mu, \theta, p)$ the reflectivity, $\epsilon(\varepsilon, \mu, \theta, p)$ the emissivity, $t(\varepsilon, \mu, \theta, p)$ the transmissivity, $T_{rec}(\varepsilon, \mu, \theta, p)$ the received temperature, T_{ill} the temperature of the illumination, T_{obj} the temperature of the object and T_{back} the temperature of the background.

In practise, the effect of the sensor cannot be neglected since it introduces noise due to scanning and interpolation. Moreover, the illumination is partially coherent which introduces some multiplicative speckle noise.

5.2. MILLIMETRE-WAVE IMAGE SIMULATION

As mentioned in Sect. 5.1, the scene is defined as an indoors environment where the illumination is incoherent. Hence, millimetre-wave images are formed due to the addition of the fluxes which are present in the scene:

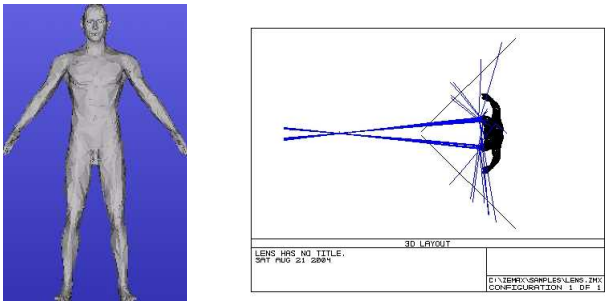

(a) (b)

Figure 8. The scene is composed basically of a body, a lens and an image plane. (a) represents the CAD model used to model the body, and (b) the position of the various objects in the scene. Note that the rays are defined to pass through the centre of the lens, avoiding noise and aberrations.

- the flux radiated by the objects (body, weapons, etc.), ϵT_{obj}
- the flux radiated by the source and reflected by the objects, RT_{ill}
- and the fluxes transmitted through the scene objects, tT_{back}.

The objective of the simulation of millimetre-wave images is therefore to model the combination of these fluxes in order to obtain synthetic millimetre-wave images, as well as the effects that the sensor has in the formation of these images. It is important to note at this point that the effects of sensor will not be taken into account since it was considered, in a first stage, as ideal, that is with no introduction of noise or aberrations. The only effect considered in order to give more realism to synthetic images is the point spread function of the system. In future versions of the simulator, real effects of the sensor will be taken into account.

The scene is composed of a body and one or several threats (weapons, knives, explosives, etc.). Each of these objects is modelled according to their physical characteristics. For instance, the body is incorporated as a CAD model (Fig. 8(a)) and threats as metallic or dielectric patches over the body. The physical characteristics of the different materials are presented in Table 1.

Table 1. Physical object characteristics

	Dielectric constant	**Physical temperature (K)**
Body		
Salty water	$\varepsilon_{body} = 27.63 + i\,33.87$	310
Threats		
Metal	$\varepsilon_{metal} = 1 + i\,5.1 \cdot 10^6$	308
Plastic	$\varepsilon_{plastic} = 2.2$	308

With regard to the sensor, the only effect taken into account is the incoherent point spread function. Since the aperture is circular, this function is ideally modelled as the Airy function.[14]

The definition and dimensions of the scene are provided in Fig. 8(b) and Table 2.

Two software tools have been used to carry out the simulation of millimetre-wave images. In the one hand, a ray-tracing programme, *Zemax*, is used to propagate rays back from each detector pixel via reflections from scene components to the source. All reflections and multiple reflections within the scene are determined using

Table 2. Dimensions of the scene

Description	**Length (m)**
Range object - closest part of the imager	1.6
Range object - apeture	2.9
Focal length	0.8
Lens diameter	1.6
Height of the body	1.8
Dimensions of the threat	0.075×0.075

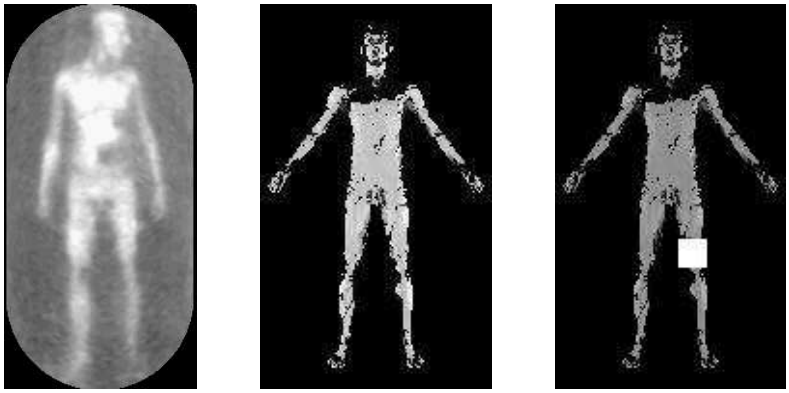

(a) (b) (c)

Figure 9. Results from the simulation: (a) real image, (b) simulated image without metal square and (c) simulated image with metal square. Note that in the simulated images noise effects are not present whereas in the real images they are. Also note that the highest temperature in the real image is smaller than in the simulated one, thus introducing a difference in the range of grey levels: simulated images appear to be darker than real ones.

Zemax and the information about every ray history is stored as a text file. By repeated application of Equation 3 at each intercept of a ray with a scene component it is possible to calculate the intensity of mm-wave radiation incident occurring at each scene pixel. This component of the simulation is executed by reading the *Zemax* output text file with *Matlab* which is used to calculate the equivalent temperatures at each pixel. Convolution of these images with the imager point spread function and the addition of random Gaussian noise yields a simulation of a mm-wave image.

The results of such a simulation are presented in Fig. 9. In these images the gray levels are calculated automatically: black represents the lowest temperature while white the highest.

6. CONCLUSIONS

This paper has presented a number of image processing techniques applied to MMW images with positive results throughout. The results from the unsupervised k-Means image segmentation were good and an excellent starting point from which to build on. The one area where it fails to segment cleanly is in areas of uneven illumination, such as the side of the body during rotation. While this could be viewed as a failure it is worth noting that the final result produces an excellent indication of the areas of the body that are well illuminated. Furthermore, it was shown that using the system to detect metallic objects in the scene allowed an adaptive number of classes, resulting in good segmentation of the objects within the scene. Work on tracking and recognition will be reported in the future.

A significant problem for this application is the tracking of the human body. The work on Active Shape Models provides an alternative segmentation based on statistical learning. The advantages given a suitable training set is that it automatically fits the contour to a plausible human pose. However, testing highlighted the difficulty of providing a complete training set and alternative technique will be investigated.

The physics required for a MMW imager has been presented and the implementation of a simluator has been discussed. Initial results have been presented and in the future further work will be presented on more complex simulations.

ACKNOWLEDGMENTS

The authors would like to acknowledge the support of QinetiQ. Dr Christopher D. Haworth and Beatriz Grafulla González are supported by EPSRC Research Grant GRS/68088.

REFERENCES

1. G. N. Sinclair, R. N. Anderton, and R. Appleby, "Outdoor passive millimetre wave security screening," in *Proceedings of the 35th International Carnahan Conference on Security Technology*, pp. 172–179, IEEE, (London, UK), October 2001.
2. T. F. Cootes, G. J. Edwards, and C. J. Taylor, "Active appearance models," *IEEE Transactions on Pattern Analysis and Machine Intelligence* **23**, pp. 681–685, June 2001.
3. P. Coward and R. Appleby, "Development of an illumination chaber for indoor millimetre-wave imaging," in *Passive Millimeter-Wave Imaging Technology VI and Radar Sensor Technology VII*, R. Appleby, D. A. Wikner, R. Trebits, and J. L. Kurtz, eds., *Proceedings of SPIE* **5077**, pp. 54–61, SPIE, August 2003.
4. K. S. J. Murphy, R. Appleby, G. Sinclair, A. McClumpha, K. Tatlock, R. Doney, and I. Hutcheson, "Millimeter wave aviation security scanner," in *Proceedings of the 36th International Carnahan Conference on Security Technology*, pp. 162–166, IEEE, (London, UK), October 2002.
5. N. G. Sinclair, P. R. Coward, R. N. Anderton, R. Appleby, T. Seys, and P. Southwood, "Detection of illegal passengers in lorries using passive millimeter wave scanner," in *Proceedings of the 36th International Carnahan Conference on Security Technology*, pp. 167–170, IEEE, (London, UK??), October 2002.
6. T. Kanungo, D. M. Mount, N. S. Netanyahu, C. D. Piatko, R. Silverman, and A. Y. Wu, "An efficient k-means clustering algorithm: analysis and implementation," *IEEE Transactions on Pattern Analysis and Machine Intelligence* **24**, pp. 881–892, July 2002.
7. L. R. Rabiner, "A tutorial on hidden markov models and selected applications in speech recognition," *Proceedings of the IEEE* **77**, pp. 257–285, February 1989.
8. M.-A. Slamani and D. D. F. Jr., "Identification of weapons in concealed weapon detection data," in *Enabling Technologies for Law Enforcement and Security*, S. K. Bramble, E. M. Carapezza, and L. I. Rudin, eds., *Proceedings of SPIE* **4232**, pp. 159–166, SPIE, 2000.
9. M.-A. Slamani, P. K. Vershney, R. M. Rao, M. G. Alford, and D. Ferris, "Image processing tools for the enhancement of concealed weapon detection," in *Proceedings of the International Conference on Image Processing*, **3**, pp. 518–522, IEEE, (Kobe, Japan), October 1999.
10. T. McInerney and D. Tezopoulos, "Deformable models in medical image analysis: A survey," *Medical Image Analysis* **1**(2), pp. 91–108, 1996.
11. A. Blake and M. Isard, *Active Contours: The Application of Techniques from Graphics, Vision, Control Theory and Statistics to Visual Tracking of Shapes in Motion*, Springer-Verlag, 1999.
12. T. F. Cootes, G. V. Wheeler, K. N. Walker, and C. J. Taylor, "View-based active appearance models," *Image and Vision Computing* **20**, pp. 657–664, August 2001.
13. T. F. Cootes and C. J. Taylor, "Statistical models of appearance for computer vision," tech. rep., Wolfson Image Analysis Unit, Imaging Science and Biomedical Engineering, University of Manchester, Manchester, M13 9PT, United Kingdom, October 2001.
14. E. Hecht, *Optics*, Addison Wesley, fourth ed., 2002.